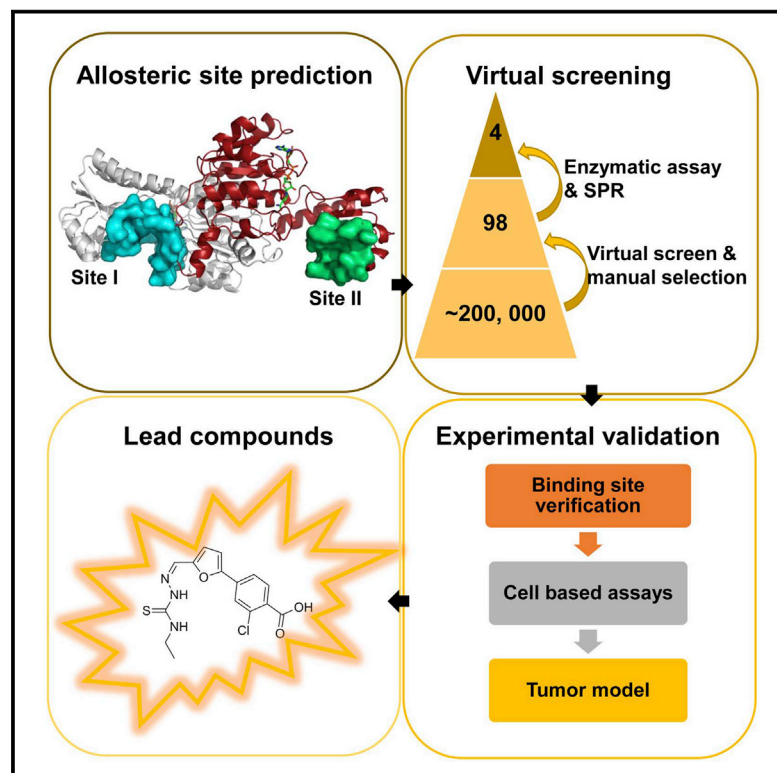


Cell Chemical Biology

Rational Design of Selective Allosteric Inhibitors of PHGDH and Serine Synthesis with Anti-tumor Activity

Graphical Abstract



Authors

Qian Wang, Maria V. Liberti, Pei Liu, Xiaobing Deng, Ying Liu, Jason W. Locasale, Luhua Lai

Correspondence

jason.locasale@duke.edu (J.W.L.),
lh lai@pku.edu.cn (L.L.)

In Brief

Wang et al. identify allosteric sites on PHGDH and discover inhibitors bound to these sites. These allosteric inhibitors are specific, bind to PHGDH in cells, reduce serine synthesis, and show anti-tumor activity in vivo.

Highlights

- Two previously unknown allosteric sites on PHGDH were identified
- Inhibitors that bind to these sites were discovered
- Inhibitors bound to PHGDH in cells and reduced the synthesis of serine and glycine
- Inhibitors suppressed tumor growth in mice

Rational Design of Selective Allosteric Inhibitors of PHGDH and Serine Synthesis with Anti-tumor Activity

Qian Wang,^{1,6} Maria V. Liberti,^{2,3,6} Pei Liu,¹ Xiaobing Deng,⁴ Ying Liu,^{1,5} Jason W. Locasale,^{2,*} and Luhua Lai^{1,4,5,7,*}

¹BNLMS, State Key Laboratory for Structural Chemistry of Unstable and Stable Species, College of Chemistry and Molecular Engineering, Peking University, Beijing 100871, China

²Department of Pharmacology and Cancer Biology, Duke Cancer Institute, Duke Molecular Physiology Institute, Duke University School of Medicine, Durham, NC 27710, USA

³Department of Molecular Biology and Genetics, Graduate Field of Biochemistry, Molecular and Cell Biology, Cornell University, Ithaca, NY 14853, USA

⁴Peking-Tsinghua Center for Life Sciences, Peking University, Beijing 100871, China

⁵Center for Quantitative Biology, Peking University, Beijing 100871, China

⁶Co-first author

⁷Lead Contact

*Correspondence: jason.locasale@duke.edu (J.W.L.), lh lai@pku.edu.cn (L.L.)

<http://dx.doi.org/10.1016/j.chembiol.2016.11.013>

SUMMARY

Metabolic reprogramming in cancer cells facilitates growth and proliferation. Increased activity of the serine biosynthetic pathway through the enzyme phosphoglycerate dehydrogenase (PHGDH) contributes to tumorigenesis. With a small substrate and a weak binding cofactor, (NAD⁺), inhibitor development for PHGDH remains challenging. Instead of targeting the PHGDH active site, we computationally identified two potential allosteric sites and virtually screened compounds that can bind to these sites. With subsequent characterization, we successfully identified PHGDH non-NAD⁺-competing allosteric inhibitors that attenuate its enzyme activity, selectively inhibit de novo serine synthesis in cancer cells, and reduce tumor growth in vivo. Our study not only identifies novel allosteric inhibitors for PHGDH to probe its function and potential as a therapeutic target, but also provides a general strategy for the rational design of small-molecule modulators of metabolic enzyme function.

INTRODUCTION

It has long been known that tumor cells exhibit altered glucose metabolism characterized by increased glucose uptake and incomplete oxidation to lactate in the presence of oxygen (Warburg, 1956; Zhao et al., 2016). With the surge of interest in understanding cancer cell metabolism, it is now widely accepted that metabolic rearrangements accompanying malignant transformation also involve numerous other pathway alterations such as the increased flux of the pentose phosphate pathway, elevated rates of lipid biosynthesis, high glutamine consumption, maintenance of redox homeostasis, and alterations in autophagy

(Pavlova and Thompson, 2016). Therefore, targeting the metabolic enzymes in these pathways provides a promising strategy for cancer therapy.

The gene encoding phosphoglycerate dehydrogenase (PHGDH), an enzyme that catalyzes the first committed step of serine biosynthesis, is also involved in metabolic reprogramming in cancer. PHGDH was identified as a focus of recurrent copy-number gain across a large set of tumors (Beroukhi et al., 2010). The *PHGDH* gene that is located at chromosome 1p12 showed copy-number gain in 16% of all cancers, including 40% of melanoma and some triple-negative breast cancers (Locasale et al., 2011; Possemato et al., 2011). Cancer cells with PHGDH amplifications are sensitive to *PHGDH* depletion, which indicates that the enzyme is required for the growth of certain tumor cells.

Recent studies have identified different regulatory mechanisms that can activate PHGDH through both transcriptional regulation and changes in its activity via posttranslational modifications (Ma et al., 2013; DeNicola et al., 2015; Ou et al., 2015; Ding et al., 2013). Additional studies have found several underappreciated functions for de novo synthesis of serine and the use of one-carbon metabolism including epigenetic maintenance and NADPH production that is important for biosynthesis and controlling the levels of reactive oxygen species (Fan et al., 2014; Mentch et al., 2015). Together these findings demonstrate that PHGDH is an attractive anti-cancer target, and that designing PHGDH inhibitors may be a fruitful enterprise.

Human PHGDH contains four domains: nucleotide-binding, substrate-binding, regulatory, and intervening domains. Currently only the crystal structure containing the first two domains is available (PDB: 2G76, Turnbull et al., 2006). The substrate-binding pocket of PHGDH is rather small, approximately 100–200 Å³, and the physiological concentration of its cofactor NAD⁺ is as high as 0.3 mM (Yamada et al., 2006). These properties likely increase the difficulties of the design of substrate-competitive inhibitors. Meanwhile, considering NAD⁺ or NADH is a widely used cofactor, which also easily causes the

problem of specificity, we focused on designing allosteric inhibitors for PHGDH that do not compete with the native ligand. Allosteric regulation can be achieved by various effectors, ranging from small molecules to macromolecules (Merdanovic et al., 2013) and can have high specificity, as allosteric binding sites are usually not evolutionarily conserved. Computational methods for rational design of allosteric effectors were emerging (Wagner et al., 2016; Ma et al., 2016) and a number of successful application examples have been reported. For example, using the two-state Go model-based allosteric site prediction method that we developed (Qi et al., 2012), we obtained novel allosteric inhibitors for *Escherichia coli* PHGDH (Wang et al., 2014). Novel enzyme activators were also found using a combined computational and experimental approach (Meng et al., 2016), providing an alternative way to control disease-related molecular networks (Pei et al., 2014).

In the present study, we first computationally identified two potential allosteric sites in PHGDH and used them to virtually screen a compound library. Selected compounds were tested for their inhibition activities using recombinant enzymes, cancer cell lines, and tumor xenograft models. Two distinct compounds with activity in cells were found. Their specificity was confirmed using a clustered regularly interspaced short palindromic repeats (CRISPR)-associated protein 9 (Cas9) gene-targeting PHGDH, chemical compound pull-down in cancer cells, and metabolomics. Recently, three studies have reported compounds that have activity against PHGDH by using high-throughput experimental screening. One series of PHGDH inhibitors showed activities in enzymatic and cell-based assays, but the binding mechanism, selectivity toward PHGDH and efficacy in vivo were unclear (Mullarky et al., 2016). Another series of inhibitors with bioactivities in enzymatic and cell-based assays, as well as a xenograft model, do not have clear binding sites (Pacold et al., 2016). The third series of inhibitors were found by a fragment screen that bind to the adenine subsite with only millimolar protein binding affinities and no further biological activities were reported (Unterlass et al., 2016). To our knowledge, the present study is the first successful example of using a structure-based approach to discover allosteric inhibitors that directly and specifically target PHGDH.

RESULTS

Allosteric Site Prediction and Identification of Novel Allosteric Inhibitors

Two potential allosteric sites, I and II, were identified computationally using a cavity detection algorithm based on defined geometric criteria (Yuan et al., 2011, 2013) (Figure 1A). Site I is close to the active site and the NAD⁺/NADH-cofactor binding site, with a volume of 847 Å³ and a predicted maximal pK_D of 8.71. It shares residues Gly78, Val79, Asp80, Asn81, and Val82 with the active site. Site II is located in the substrate-binding domain, with a volume of 463 Å³ and a predicted maximal pK_D of 7.79. Molecular docking across a large virtual compound library was then conducted (Halgren et al., 2004; Friesner et al., 2004). Ninety-eight compounds were selected and then acquired to test their abilities to regulate PHGDH activity.

PKUMDL-WQ-2101 in site I and PKUMDL-WQ-2201 to 2203 in site II were identified to significantly affect the

PHGDH activity in a concentration-dependent manner (Figures 1B and 1C, and S1A). SPECS IDs of these four compounds are shown in Table S1, and their K_D values were determined by using surface plasmon resonance (SPR) (Figures 1D, and S1B–S1G). SPR experiments also demonstrated these inhibitors did not aggregate under the experimental conditions.

To test whether the compounds indeed bind to site I and II, respectively, we selected PKUMDL-WQ-2101 in site I and PKUMDL-WQ-2201 in site II, and performed competition experiments and mutagenesis studies. The competition experiments between these compounds and cofactor NADH indicated that they did not bind in the cofactor site (Figures 1E and S1H). Inhibition ability of PKUMDL-WQ-2101 and PKUMDL-WQ-2201 for the C-terminal-truncated PHGDH containing only the substrate-binding domain and the nucleotide-binding domain demonstrated that the C-terminal regulatory and intervening domains did not contribute to binding and the compounds bound to the N-terminal domains used for virtual screening (Figures S1I and S1J). Based on the docking structures, mutants R134A and K57AT59A for PKUMDL-WQ-2101, and mutants T59A and T56AK57A for PKUMDL-WQ-2201, were made and tested (Figures 1F–1I). All these mutants retained their secondary structures (Figure S1K) and exhibited reduced responses to the corresponding inhibitors. For PKUMDL-WQ-2101, the PHGDH-inhibiting activities were dramatically reduced for mutants R134A (half maximal inhibitory concentration [IC₅₀] = 141 ± 4 μM, max inhibition = 49%) and K57AT59A (IC₅₀ = 128 ± 10 μM, max inhibition = 47%) compared with that for wild-type (WT) PHGDH (IC₅₀ = 34.8 ± 3.6 μM, max inhibition = 67%) (Figure 1G). For PKUMDL-WQ-2201, its inhibition abilities for PHGDH mutants were also significantly decreased. The IC₅₀ values for T59A and T56AK57A were 69 ± 40 μM and >300 μM, respectively, while the IC₅₀ value for WT PHGDH was 35.7 ± 8.6 μM (Figure 1I). In addition, the inhibition ability of PKUMDL-WQ-2101 to T59A and T56AK57A (key residues in site II) or the inhibition ability of PKUMDL-WQ-2201 to R134A and K57AT59A (key residues in site I) were also measured to verify the specificity of inhibitor binding (Figures 1G and 1I). These results support that PKUMDL-WQ-2101 and PKUMDL-WQ-2201 bound in site I and site II, respectively.

Combination therapy is emerging as a promising strategy to generate synergistic therapeutic effects, reduce side effects of monotherapy, overcome multidrug resistance, and reduce the dose of each drug required (Yang et al., 2015; Botham et al., 2014), which can also be used to demonstrate whether two compounds bind to the same site or to different sites. Synergism can be quantified through the calculation of combination indices (Chou, 2006). When the concentration of PKUMDL-WQ-2101 was kept at 25 μM (approximate IC₅₀ value), synergistic interactions were observed with PKUMDL-WQ-2201 concentrations ranging from 1 to 200 μM (Figures 1J and S2A). In contrast, when the concentration of PKUMDL-WQ-2202 was kept at 25 μM, PKUMDL-WQ-2201 and PKUMDL-WQ-2202 showed antagonism rather than synergy, indicating that they compete for a single site (Figures 1J and S2B). Together, these synergistic results further confirm our docking results about the binding sites of the compounds.

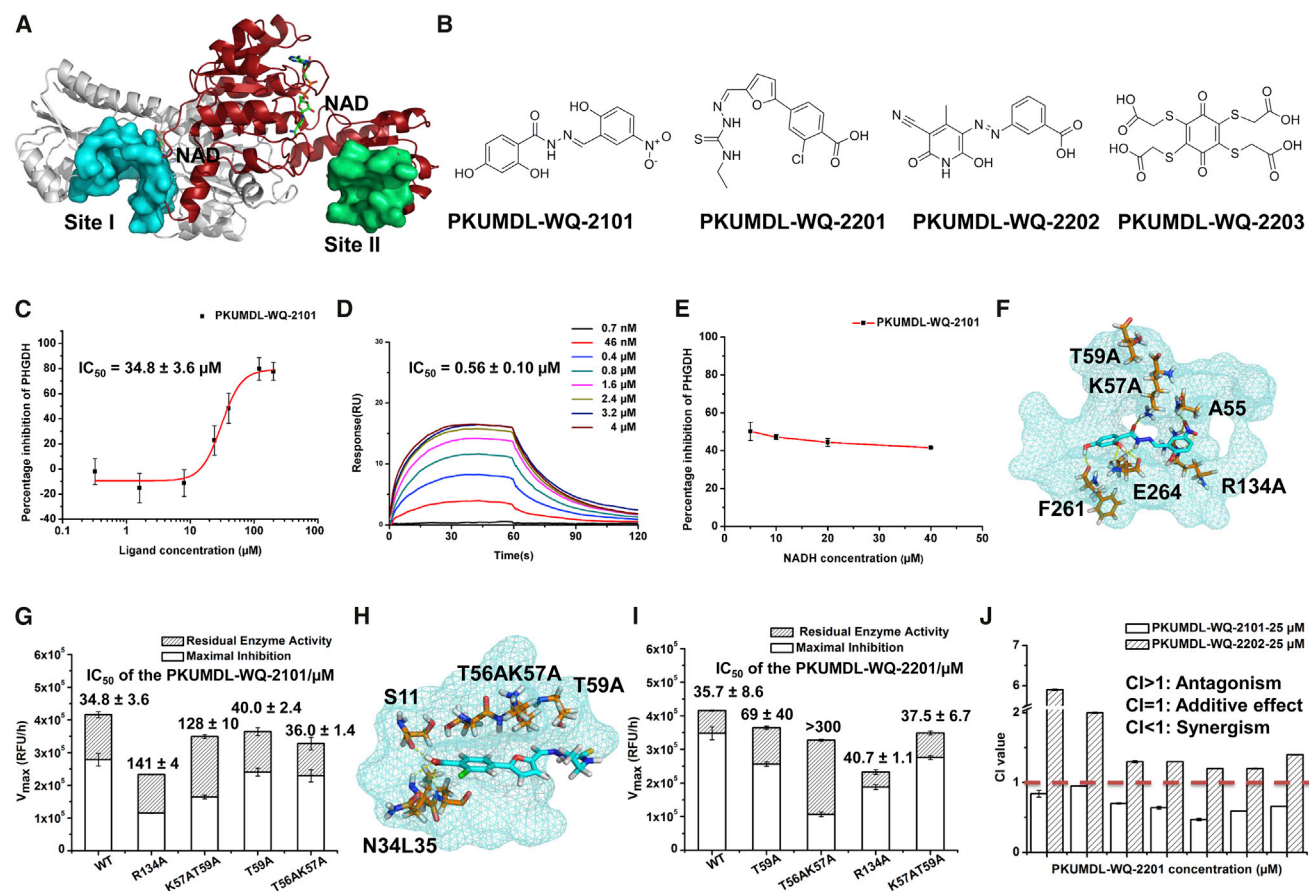


Figure 1. Identification of Novel Allosteric Inhibitors of PHGDH

(A) Potential allosteric sites in PHGDH (PDB: 2G76). The sites were predicted by the program CAVITY and illustrated using the surface mode. The cofactor NAD⁺ is indicated in sticks. PHGDH forms a dimer in the crystal structure, sites I and II exist in each monomer, and only one site I and one site II are shown in the figure for clarity.

(B) Chemical structures of PHGDH inhibitors.

(C) Enzyme inhibition dose-response curve of PKUMDL-WQ-2101.

(D) SPR dose-response curve of PKUMDL-WQ-2101.

(E) Cofactor competition curve of PKUMDL-WQ-2101. The percentage inhibition did not obviously change along with the increase of NADH concentration, indicating that there are no significant interactions between PKUMDL-WQ-2101 and the cofactor binding site.

(F–G) Predicted binding mode of PKUMDL-WQ-2101. The compound and key residues in site I are shown in stick representation. Site I is shown in surface mode (F). Enzymatic activities and responses to PKUMDL-WQ-2101 of PHGDH mutants (G).

(H–I) Predicted binding mode of PKUMDL-WQ-2201. The compound and key residues in site II are shown in stick representation. Site II is shown in surface mode (H). Enzymatic activities and responses to PKUMDL-WQ-2201 of PHGDH mutants (I).

(J) Inhibitors in different sites synergize to induce PHGDH inhibition. The concentration of PKUMDL-WQ-2101 and PKUMDL-WQ-2202 was kept at 25 μM for enzyme inhibition assay, while PKUMDL-WQ-2201 concentration varies. Combination index (CI) values < 1 indicate synergistic interaction. Data shown represent the mean ± SD (n = 3). See Figure S1 for dose-response curves of PKUMDL-WQ-2201 to 2203 and Figure S2 for synergistic matrix.

Cellular Effects of PKUMDL-WQ-2101 and PKUMDL-WQ-2201

The effects of the compounds against a panel of cancer cell lines along with one immortalized human breast epithelial cell line were evaluated. PKUMDL-WQ-2101 and PKUMDL-WQ-2201 showed dose-dependent suppression effects on the cell viability at micromolar concentrations, with good selectivity for PHGDH-amplified breast cancer cell lines (Figures 2A and 2B), while PKUMDL-WQ-2202 and PKUMDL-WQ-2203 showed weak bioactivities in cell-based assays with half maximal effective concentration (EC₅₀) values more than 200 μM (Figure S3). The antitumor activities of PKUMDL-WQ-2101 in the two PHGDH-

amplified breast cancer cell lines (MDA-MB-468 and HCC70) were 7.70 and 10.8 μM, which were 3- to 4-fold, 8- to 12-fold, and 14- to 20-fold more active than its antitumor activities in PHGDH non-dependent cell lines, MDA-MB-231, ZR-75-1, and MCF-7 cell lines, respectively. For PKUMDL-WQ-2201, the EC₅₀ values were 6.90 μM in MDA-MB-468 and 10.0 μM in HCC70 cell lines, which were 13- to 18-fold more active than that of ZR-75-1. No bioactivities in the other three PHGDH non-amplified breast cancer cell lines tested were measurable. Meanwhile, PKUMDL-WQ-2101 and PKUMDL-WQ-2201 exerted weak cytotoxic effects on the MCF-10A cell line, which was consistent with previous observations of PHGDH

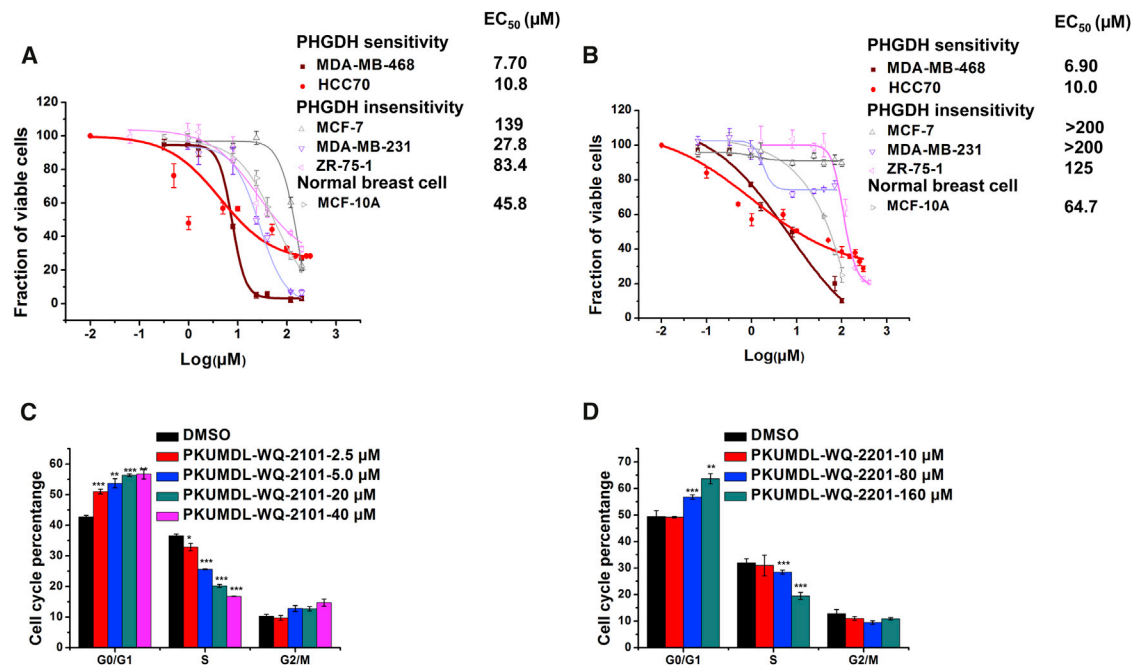


Figure 2. Bioactivities of PKUMDL-WQ-2101 and PKUMDL-WQ-2201 in Cell-Based Assays

(A and B) Growth inhibition activity of PKUMDL-WQ-2101 (A) and PKUMDL-WQ-2201 (B) in MDA-MB-468, HCC70, MCF-7, MDA-MB-231, ZR-75-1, and MCF-10A cells, respectively. Cells were exposed to vehicle or various concentrations of PKUMDL-WQ-2101 or PKUMDL-WQ-2201 for 72 hr followed by MTT assay. (C and D) Percentage of MDA-MB-468 cells in different phases of the cell cycle after treatment, respectively, with 2.5, 5.0, 20, and 40 μM PKUMDL-WQ-2101 (C) and 10, 80, and 160 μM PKUMDL-WQ-2201 (D) for 24 hr. DMSO was used as vehicle. Data represent the mean ± SD independent experiments. Difference is significant by two-tailed multiple t test, * $p < 0.05$, ** $p < 0.01$, *** $p < 0.001$. See Figure S3 for cell bioactivities of PKUMDL-WQ-2202 and 2203.

requirements using genetic approaches (Locasale et al., 2011). The antitumor activities of PKUMDL-WQ-2101 and PKUMDL-WQ-2201 against MDA-MB-468 cells may be caused by their influence on cell cycle (Figures 2C and 2D).

Compound Activity is Selective for PHGDH

To further evaluate the activity and selectivity of the compounds, we developed a CRISPR-Cas9-mediated *PHGDH* gene knockout (KO). We designed a single-guide RNA (sgRNA) with a protospacer adjacent motif sequence specifically targeting a coding region in exon 8 of the *PHGDH* gene, predicted to result in a frameshift mutation and loss of function (Shalem et al., 2014; Mali et al., 2013) (Figure 3A). A clonal population of SKOV3 ovarian cancer cells was obtained and able to grow in the absence of *PHGDH*. Complete KO was confirmed with immunoblotting in reference to a cell line created by targeting a sgRNA against *GFP* (Figure 3B). A 6-day growth curve revealed the ability of *PHGDH* KO cells to grow, albeit more slowly than the *GFP* KO control cells ($p < 0.01$, two-tailed multiple t test) (Figure 3C). We then evaluated the compounds PKUMDL-WQ-2101 and PKUMDL-WQ-2201 on these cell lines. The *GFP* KO cells exhibited sensitivity to PKUMDL-WQ-2101 ($IC_{50} = 37.3 \mu M$) (Figure S4A) and, albeit to a lesser extent to PKUMDL-WQ-2201 ($IC_{50} = 291.53 \mu M$) (Figure S4B). To further understand the specificity of these compounds, 6-day proliferation assays were carried out in SKOV3 control and *PHGDH* KO cells. *GFP* KO cell growth was significantly suppressed after treatment with PKUMDL-WQ-2101 ($p < 10^{-3}$, two-tailed Student's t test) (Fig-

ure 3D), whereas *PHGDH* KO cells were able to proliferate in the presence of the compound (Figure 3E). Similarly, albeit to a lesser extent, proliferation in SKOV3 control cells was suppressed after 6 days in the presence of PKUMDL-WQ-2201 ($p < 0.05$, two-tailed Student's t test) (Figure 3F), whereas *PHGDH* KO cell growth remained unaffected ($p > 0.99$, two-tailed Student's t test) (Figure 3G). Chemical compound pull-down assays were also carried out to verify PKUMDL-WQ-2101 with the best binding affinity was specifically bound to *PHGDH* in MDA-MB-468 cells (Figures S4C–S4E). These results indicated that the cytotoxicity to these compounds appears to a large extent specific to *PHGDH* and serine synthesis.

We then investigated the effects of *PHGDH* KO on serine metabolism. Liquid chromatography coupled to high-resolution mass spectrometry (LC-HRMS) and stable isotope labeling were used to monitor the conversion of uniformly labeled $U-^{13}C$ -glucose to metabolites in the serine metabolic network in both SKOV3 *GFP* KO control and SKOV3 *PHGDH* KO cells (Figure 4A). We detected ^{13}C -glucose incorporation in both serine and glycine in SKOV3 *GFP* KO cells, but not in SKOV3 *PHGDH* KO cells, confirming that the knockout fully abrogated de novo serine synthesis (Figure 4B). Both compounds (about IC_{50}) also produced comparable metabolic effects on the serine metabolic network and reduced glucose incorporation into serine and glycine metabolites by more than 50% (Figures 4C and 4D). We further investigated pathways downstream of serine upon inhibition of *PHGDH* with PKUMDL-WQ-2101 and PKUMDL-WQ-2201. Given that serine is essential for

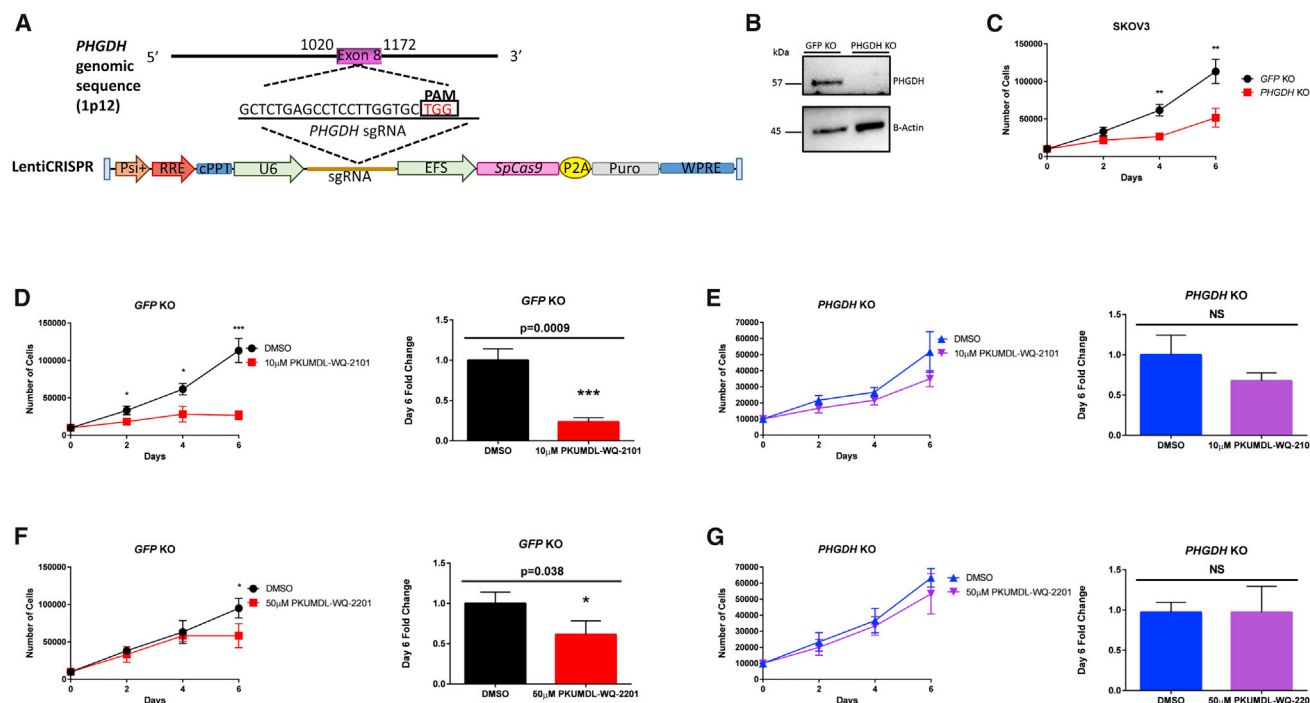


Figure 3. CRISPR-Cas9-Mediated *PHGDH* KO and *PHGDH* Inhibition by PKUMDL-WQ-2101 and PKUMDL-WQ-2201

(A) Overview of the lentiCRISPR system and sgRNA design generated for targeted *PHGDH* deletion in SKOV3 ovarian cancer cells.

(B) Western blot analysis for SKOV3 GFP KO control and SKOV3 *PHGDH* KO cells with actin as a loading control.

(C) Growth curve comparing SKOV3 GFP KO control and *PHGDH* KO over 6 days.

(D) Growth curves of SKOV3 GFP KO control and (E) *PHGDH* KO cells after 6 days of treatment with vehicle or 10 μ M PKUMDL-WQ-2101 followed by cell counting.

(F) Growth curves of SKOV3 GFP KO control or (G) *PHGDH* KO cells after 6 days of treatment with vehicle or 50 μ M PKUMDL-WQ-2201 followed by cell counting. All values represent the mean \pm SEM from $n = 3$ biological replicates.

p Values were obtained from a two-tailed Student's *t* test, * $p < 0.05$, ** $p < 0.01$, *** $p < 0.001$. See Figure S4 for PKUMDL-WQ-2101 and 2201 bioactivities on SKOV3 GFP KO cells and results of PKUMDL-WQ-2101 pull-down assays.

nucleotide synthesis (Locasale, 2013), we investigated whether ^{13}C -glucose consumption into nucleotides was altered after treatment. We analyzed the mass isotopomer distribution (MID) of one pyrimidine and purine synthesis by measuring uridine triphosphate (UTP) and ATP, and determined whether a difference in the mass shift of 1 or 2 ($m + 1$ or $m + 2$), known to result from incorporation of serine or glycine, was observed. We also monitored any changes in $m + 6$ or $m + 7$, which correspond to labeling from both the pentose phosphate and serine biosynthesis pathways. Upon treatment with both PKUMDL-WQ-2101 and PKUMDL-WQ-2201, decreases in $m + 2$, $m + 6$, and $m + 7$ glucose labeling were observed in UTP and ATP, indicating a direct effect of *PHGDH* inhibition on nucleotide synthesis (Figures 4E and 4F). A sharp decrease in the $m + 5$ peak was also observed due to a decrease in ribose labeling from the pentose phosphate pathway, suggesting that *PHGDH* ablation likely exerts effects on nucleotide synthesis through affecting glycolysis or occurs indirectly as a product of on-target cytotoxicity of the compound. We excluded interpretation of the $m + 1$ peak due to the confounding influence of natural abundance isotopes. We also analyzed glucose incorporation into glutathione, another metabolite belonging to a pathway downstream of serine and glycine synthesis, and decreases in $m + 2$ were found in cells treated with both compounds (Figure 4G). These data suggest

that *PHGDH* inhibition by PKUMDL-WQ-2101 and PKUMDL-WQ-2201 decreases de novo serine synthesis and metabolism downstream of the serine synthesis pathway, with effects comparable with *PHGDH* genetic deletion.

PKUMDL-WQ-2101 and PKUMDL-WQ-2201 Inhibits Tumor Growth of Amplified Cell Lines In Vivo

Previous studies have questioned whether *PHGDH* inhibition is required for longer-term tumor maintenance (Chen et al., 2013). To further understand the role of *PHGDH* in tumor growth and maintenance in vivo, MDA-MB-468 and MDA-MB-231 cells were injected into the fourth mammary pad of non-obese diabetic (NOD).CB17 severe combined immunodeficiency (SCID)/J mice. Tumor volumes were monitored every 2 days. We found that both PKUMDL-WQ-2101 and PKUMDL-WQ-2201 exhibited substantial inhibitory effects on MDA-MB-468 xenografts compared with vehicle-treated mice after 30 days of drug delivery (Figure 5). For MDA-MB-231 xenografts, neither PKUMDL-WQ-2101 nor PKUMDL-WQ-2201 affected tumor growth (Figure S5A and S5B), further confirming the specificity of the compounds. The compounds appeared to also be tolerated as all mice were able to maintain normal body weight over the course of the experiments (Figures S5C–S5E). Although the two compounds synergized each other to potentially induce

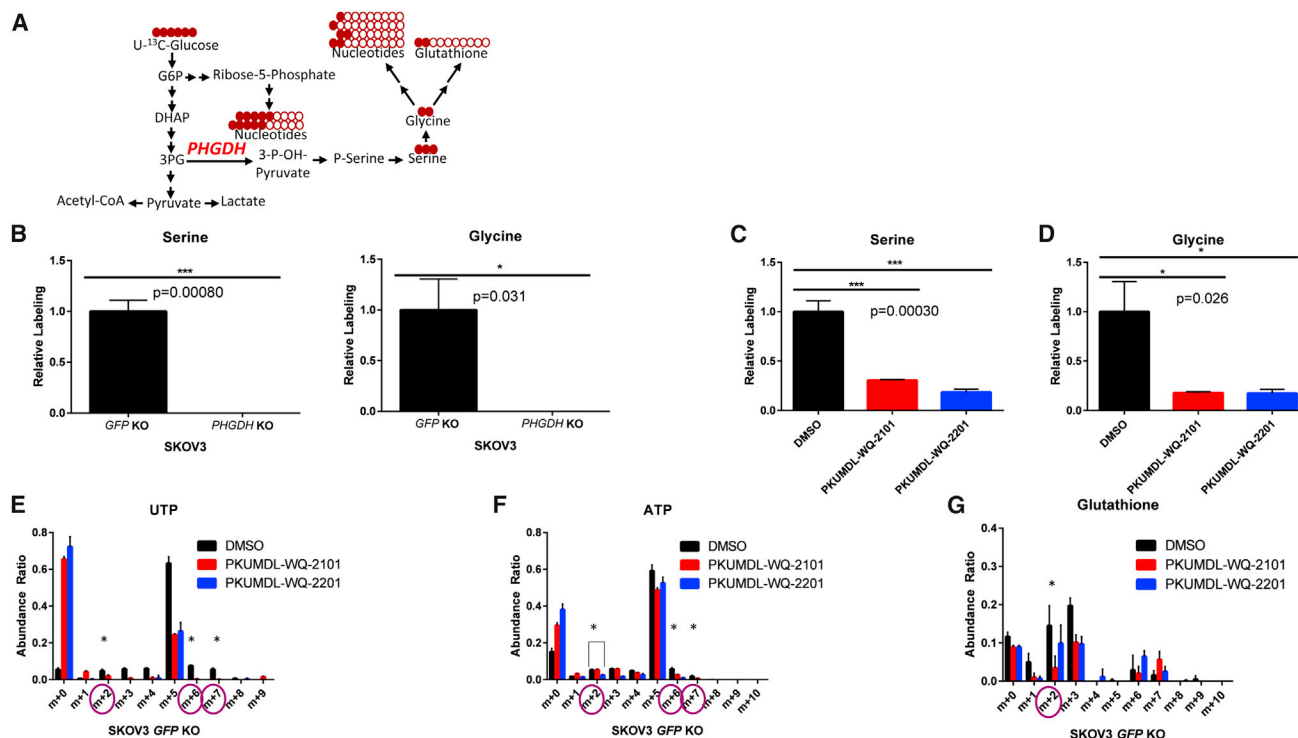


Figure 4. PKUMDL-WQ-2101 and PKUMDL-WQ-2201 Inhibit the Serine Biosynthesis Pathway in Cells

(A) Schematic of U-¹³C-glucose stable isotope labeling used to detect carbon labeling from glucose (red) in metabolites part of the serine metabolic network. (B–D) ¹³C-serine and ¹³C-glycine labeling from glucose in SKOV3 GFP KO control cells (B) compared with SKOV3 PHGDH KO cells after 24 hr ¹³C-serine (C) and ¹³C-glycine labeling (D) from glucose in SKOV3 GFP KO cells after 24 hr treatment with 37 μ M PKUMDL-WQ-2101 and 291 μ M PKUMDL-WQ-2201, followed by subsequent U-¹³C-glucose labeling.

(E and F) MID of UTP (E) and ATP (F) after 24 hr treatment with 37 μ M PKUMDL-WQ-2101 and 291 μ M PKUMDL-WQ-2201, followed by subsequent U-¹³C-glucose labeling.

(G) Glutathione after 24 hr treatment with 37 μ M PKUMDL-WQ-2101 and 291 μ M PKUMDL-WQ-2201, followed by subsequent U-¹³C-glucose labeling. All values represent the mean \pm SEM from n = 3 biological replicates.

Difference is significant by one-way ANOVA, *p < 0.05, ***p < 0.001.

enzyme activity inhibition, the combination strategy was not applied to the mouse model, due to the complicated pharmacokinetic issues of in vivo compound concentration and clearance time, which may not exactly match. Nevertheless, these findings confirm the bioactivity, tolerability, and selectivity for PHGDH in vivo.

DISCUSSION

Using a structure-based drug design approach, we successfully identified compounds that bound to the predicted allosteric sites and effectively inhibited the enzyme activity of PHGDH. These compounds exhibited sub-micromolar to micromolar binding affinities and inhibited cancer cell growth in the micromolar range. PKUMDL-WQ-2101 and PKUMDL-WQ-2201 showed good activity and selectivity to PHGDH overexpression breast cancer cells. The use of CRISPR-Cas9-mediated PHGDH KO in SKOV3 cells provided a genetic evaluation of the relative on- and off-target effects of each compound, whereby PKUMDL-WQ-2101 had high selectivity for PHGDH control, but not KO cells. PKUMDL-WQ-2101 and PKUMDL-WQ-2201 were proven to suppress PHGDH-amplified breast cancer cell growth in mice. Our study provides the first success-

ful example of PHGDH allosteric inhibitor discovery using a structure-based approach.

The identified PKUMDL-WQ-2101 and PKUMDL-WQ-2201 compounds are novel allosteric inhibitors for PHGDH with unique structures. No biological activities for these compounds have been reported before. Although PKUMDL-WQ-2101 was predicted as a pan-assay interference compound (Baell and Holloway, 2010), due to the hydroxyl-phenyl-hydrazone group in its structure, the promiscuity has been eliminated by changing ionic strength or adding DTT in the enzymatic assay, SPR, and mutagenesis experiments, because the hydroxyl-phenyl-hydrazone group was generally believed to have the tendency for aggregation (McGovern et al., 2002), spectroscopic absorption (Auld et al., 2008), chelation (Ainscough et al., 1999), and reactivity, thus being inactive proteins. In addition, the catalytic process of PHGDH or PSAT1 does not need the participation of metal ions, and PKUMDL-WQ-2101 showed good selectivity to PHGDH-amplified breast cancer cells. Furthermore, PKUMDL-WQ-2101 showed bioactivity in vivo, confirming that PHGDH is required for tumor maintenance. These experimental results confirmed that PKUMDL-WQ-2101 specifically bound to PHGDH and inhibited its enzymatic activity.

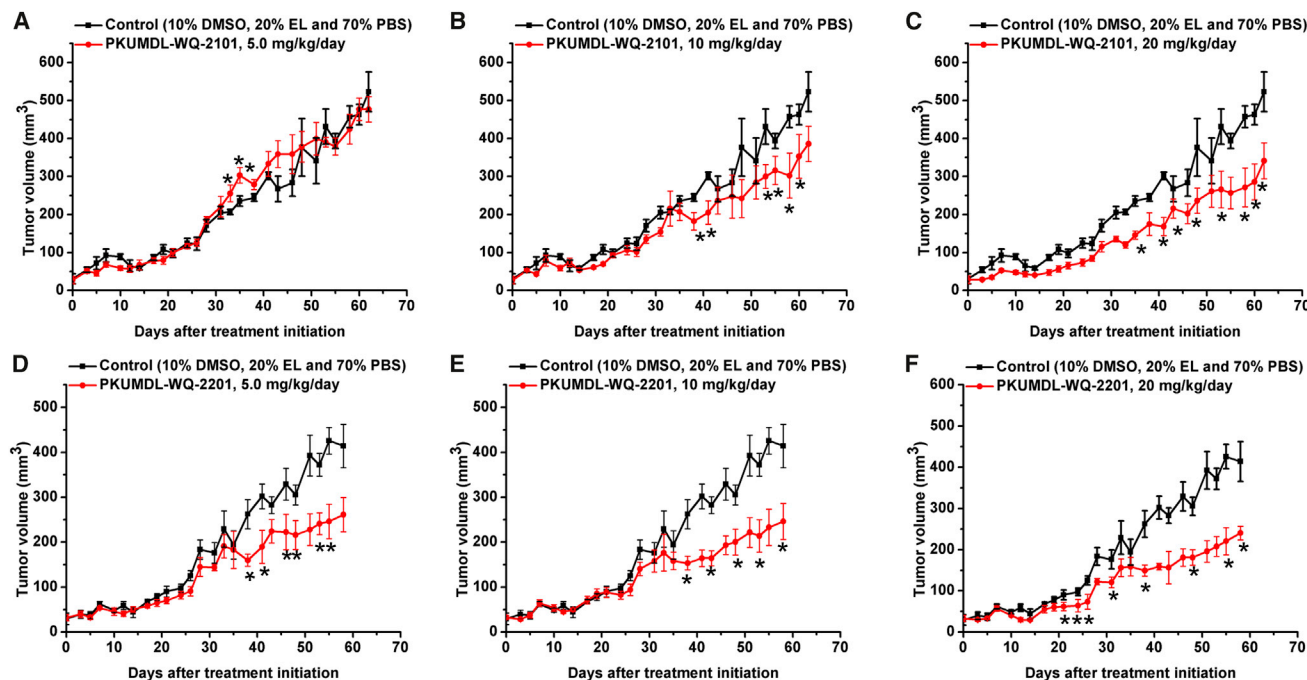


Figure 5. Bioactivities of PKUMDL-WQ-2101 and PKUMDL-WQ-2201 In Vivo

(A–F) After 30 days of drug delivery, treatment with PKUMDL-WQ-2101 (A)–(C) or PKUMDL-WQ-2201 (D)–(F) significantly suppressed the growth of tumors compared with the control-treated group. Data represent the mean \pm SEM of independent experiments. Difference is significant by two-tailed multiple t test, $p < 0.05$. See Figure S5 for PKUMDL-WQ-2101 and 2201 bioactivities on MDA-MB-231 xenografts and mouse growth curves.

Allosteric regulation needs communication between the allosteric site and the distant functional site. Therefore, the high binding affinity of allosteric ligands may not necessarily cause a strong influence on protein function (Nussinov and Tsai, 2014). In the case of PKUMDL-WQ-2101, while its K_D value is $0.56 \pm 0.10 \mu\text{M}$, its PHGDH inhibition activity IC_{50} value is $34.8 \pm 3.6 \mu\text{M}$. Previous studies showed that a large number of protein conformations in solution pre-exist and can be characterized by the energy landscape (Kar et al., 2010). Allosteric effectors may change the distribution of these conformations. PKUMDL-WQ-2101 and PKUMDL-WQ-2201 inhibited PHGDH activity mainly by forming hydrogen-bond networks with sites I and II, respectively, limiting the movement of the rigid domains, preventing the active sites from closing, thus stabilizing PHGDH in the inactive conformation. Nevertheless, further experimental or computational studies are needed to better understand this inhibitory mechanism.

Three recent studies have reported compounds with activities against PHGDH. One study reported an example of a PHGDH inhibitor by screening a library of 800,000 drug-like compounds (Mullarky et al., 2016). The best compound, CBR-5884 inhibited PHGDH enzymatic activity with an IC_{50} of $33 \pm 12 \mu\text{M}$ in a time-dependent manner. CBR-5884 was speculated as a covalent inhibitor binding to a Cys in the non-active site and disrupting the enzyme oligomerization state. At $30 \mu\text{M}$, CBR-5884 inhibited the growth of MDA-MB-468 cells by 35%–60% in serine-replete medium, and by 80%–90% in serine-deplete medium. Neither a direct binding test nor a postulated binding site was reported. CBR-5884 was unstable in mouse plasma and could not be used for in vivo testing. Another study reported three PHGDH in-

hibitors by first screening a 400,000-compound NIH Molecular Libraries Small Molecule Repository library and then optimizing the lead compounds (Pacold et al., 2016). The best compound, NCT-503, exhibited an IC_{50} value of $2.5 \pm 0.6 \mu\text{M}$ and showed some selectivity in PHGDH-amplified breast cancer cell lines and had bioactivities in a xenograft model. Although NCT-503 was found to not be substrate competitive, its specific binding site remains unknown. The third study reported 15 fragments with PHGDH inhibition activities by first screening a library of 600 fragments, then validating the fragments by using the thermal shift assay, isothermal titration calorimetry competition experiments, and X-ray crystallography (Unterlass et al., 2016). All the 15 fragments bound in the adenine subsite with millimolar binding affinities. However, fragment activities in cells and tumors were not reported. In the present study, we successfully discovered novel allosteric inhibitors for PHGDH using a structure-based design approach with the best IC_{50} of $28.1 \pm 1.3 \mu\text{M}$ for enzyme inhibition. PKUMDL-WQ-2101 and PKUMDL-WQ-2201 were confirmed to specifically bind to PHGDH in PHGDH-amplified breast cancer cells with EC_{50} values less than $10 \mu\text{M}$ in serine-replete medium, which was better than that of CBR-5884 and similar to that of NCT-503. Furthermore, PKUMDL-WQ-2101 and PKUMDL-WQ-2201 also suppressed tumor growth in mice. We started from purposely designing allosteric inhibitors for the predicted allosteric sites, while CBR-5884 and NCT-503 were found from high-throughput screening. Nevertheless, all the compounds inhibit PHGDH by an allosteric effect, demonstrating that allosteric inhibition is a promising strategy to suppress its activity. More allosteric inhibitors for PHGDH can be expected in the future.

In the past decade, considerable efforts have been devoted to identify agents to suppress oncogenesis and tumor progression (Hanahan and Weinberg, 2011), and then develop drugs to selectively kill cancer cells based on their metabolic alterations. Several drug candidates were successfully discovered and entered into clinic trials, such as AZD3965 (Birsoy et al., 2013; Sonveaux et al., 2008) and TCD-717 (Clem et al., 2011). Some anti-metabolite agents have even been used in a clinical setting for a long time, such as 5-fluorouracil, methotrexate, and gemcitabine (Galluzzi et al., 2013). We are hopeful that PKUMDL-WQ-2101 and PKUMDL-WQ-2201 may be an additional starting point to further target cancer metabolism. In conclusion, we have successfully discovered PHGDH allosteric inhibitors targeting the predicted allosteric sites by using virtual screening and experimental validation. The compounds reported can be further optimized and developed for next-generation anti-cancer therapies.

SIGNIFICANCE

Cancer cells reprogram metabolism to support their growth and proliferation. During the past decades, targeting cancer metabolism has emerged as a promising strategy for the development of selective anti-cancer agents. The gene encoding phosphoglycerate dehydrogenase (PHGDH), an enzyme that catalyzes the first critical step of serine biosynthesis, is involved in metabolic reprogramming in cancer. The *PHGDH* gene that is located at chromosome 1p12 showed copy-number gain in 16% of all cancers including 40% of melanoma and some triple-negative breast cancers. Cancer cells with PHGDH amplifications are sensitive to PHGDH depletion, which indicates that the enzyme is required for the growth of certain tumor cells. Although the importance of PHGDH as a cancer target has been proposed, the lack of small-molecule inhibitors hinders further exploration. The high cellular concentration and wide use of its cofactor (NAD^+) and the small size of the active site make inhibitor discovery of targeting the active site difficult. We used a computational approach to scan for possible allosteric sites and used them to virtually screen for allosteric inhibitors. Two novel allosteric sites on PHGDH were identified. Compounds that directly bind to these sites, inhibit PHGDH enzyme activity, suppress cancer cell proliferation and in vivo tumor growth were found. The best compound binds to PHGDH with a dissociation constant of 0.56 μM , which selectively inhibits a PHGDH-amplified breast cancer cell line with EC_{50} value less than 10 μM . The inhibitors were also characterized using metabolomics on PHGDH-amplified, CRISPR-Cas9-generated *PHGDH* knockout cell lines, and mice to demonstrate the specificity and activity in vivo. Our study not only identifies novel allosteric inhibitors for PHGDH with in vivo activity to probe its function and potential as a therapeutic target, but also provides a general strategy for the rational design of small-molecule modulators of metabolic enzyme function.

EXPERIMENTAL PROCEDURES

Allosteric Site Prediction and Virtual Screening

Potential allosteric sites in the PHGDH N-terminal fragment structure containing the substrate-binding and nucleotide-binding domains (PDB: 2G76) were

identified using the CAVITY program (Yuan et al., 2011, 2013) and then applied to screen for potential allosteric inhibitors. The program Glide Standard Precise (SP) mode and Extra Precise (XP) mode were used to do the molecular docking studies and screen the SPECS library (Friesner et al., 2004; Halgren et al., 2004). The top 5% compounds from the XP mode were chosen for manual selection and purchased from SPECS for experimental testing.

Molecular Cloning, Protein Expression, and Purification

The full-length *PHGDH* (Genbank: NM_006623) or PSAT1 (Genbank: NM_021154) open reading frame (Seajet Scientific) was amplified by PCR, ligated into the pET21a(+) vector, transformed to the BL21 (DE3) strain of *E. coli*, and purified using a nickel-nitrilotriacetic column (HisTrap HP; GE Healthcare), and then a gel-filtration column (Sephacryl S-200 HR, GE Healthcare). For details, see Supplemental Experimental Procedures.

Enzyme Assay

Due to the unavailability of PHGDH direct-substrate phosphohydroxypyruvate, the enzyme activity of PHGDH was measured accompanied by the upstream PSAT1 catalytic reaction (Hart et al., 2007). For details, see Supplemental Experimental Procedures.

SPR Experiments

The binding affinities of compounds toward PHGDH were assayed using the SPR-based Biacore T200 instrument (GE Healthcare). PHGDH was immobilized on a CM5 sensor chip using standard amine-coupling at 25°C with 1× running buffer PBS-P (GE Healthcare), as described previously (Wang et al., 2014). For details, see Supplemental Experimental Procedures.

Competition Experiments

To investigate competition effects between the compounds and the cofactor NADH, we performed compound-cofactor competition experiments as follows: before pSer was added to start the reaction, the enzyme sample was pre-incubated with cofactor and the compound for 10 min at 25°C. The compound was kept at a constant inhibitory concentration (50 μM), while the NADH concentration was gradually increased from 5 to 40 μM . At these concentrations, the compounds inhibited PHGDH activity by ~50% when the NADH concentration was 150 μM .

Mutagenesis Experiments

All mutagenesis experiments were carried out according to the instructions for QuikChange Site-Directed Mutagenesis (SBS Genetech). The plasmid pET-21a(+)-containing WT PHGDH was mutated to obtain the mutants. The DNA sequences of all mutants were verified by DNA sequencing. The protein expression and activity assays of the mutants were performed as described for the WT.

Cell Culture

MDA-MB-468, MDA-MB-231, and ZR-75-1 from the China Infrastructure of Cell Line Resources, and SKOV3 and HCC70 from the American Type Culture Collection (ATCC), were maintained in RPMI-1640 culture medium (Gibco) supplemented with 10% fetal bovine serum and 1% penicillin/streptomycin/mL. MCF-7 from the China Infrastructure of Cell Line Resources and HEK293T from the ATCC were maintained in DMEM (Gibco) supplemented with 10% fetal bovine serum and 1% penicillin/streptomycin/mL. MCF-10A from the China Infrastructure of Cell Line Resources was maintained in DMEM/F12 (1:1) medium (Gibco) and supplemented with 5% horse serum, 10 $\mu\text{g/mL}$ insulin, 0.1 $\mu\text{g/mL}$ cholera toxin, 0.5 $\mu\text{g/mL}$ hydrocortisone, and 0.02 $\mu\text{g/mL}$ epidermal growth factor.

Proliferation Assays

SKOV3 GFP KO and *PHGDH* KO cells (10,000 cells/well) were plated into 24-well culture plates in triplicate. After 24 hr, cells were treated with DMSO or compound. Each day, cells were counted by the trypan blue exclusion test for cell viability at a 1:1 ratio using a hemocytometer.

MTT Assays

MDA-MB-468 (5,000 cells/well), HCC70 (5,000 cells/well), MCF-7 (3,000 cells/well), MDA-MB-231 (2,000 cells/well), ZR-75-1 (4,000 cells/well), and

MCF-10A (3,000 cells/well) in exponential growth were plated into 96-well culture plates and allowed to adhere overnight. The number of viable cells was assessed by spectrophotometry at 490 nm using a BioTek Synergy4 Microplate Reader after 3 days treatment, and calculated as the percentage of absorbance of treated cells relative to that of solvent controls.

For SKOV3 WT/KO cells (30,000 cells/well) were plated in a 96-well plate. The following day, the medium was aspirated and replaced with 100 μ L of phenol red-free RPMI-1640 (Gibco), and 12 mM methyl thiazolyldiphenyl-tetrazoliumbromide (MTT, Thermo Fisher Scientific) was added to the cells. After 4 hr, the medium containing MTT was aspirated and 50 μ L of DMSO was added to dissolve the formazan and read at 540 nm.

Synergistic Experiments in Enzymatic Assays

For the combination of PKUMDL-WQ-2101 and PKUMDL-WQ-2201, one concentration among 0, 1, 5, 12.5, 25, 50, 100, 200 μ M of PKUMDL-WQ-2101 was successively mixed with different concentrations of PKUMDL-WQ-2201 (0, 1, 5, 12.5, 25, 50, 100, 200 μ M), and the mixture was then pre-incubated with enzyme samples to test their effects on PHGDH activity.

For the combination of PKUMDL-WQ-2201 and PKUMDL-WQ-2202, one concentration among 0, 1, 5, 12.5, 25, 50, 100, 200 μ M of PKUMDL-WQ-2201 was successively mixed with different concentrations of PKUMDL-WQ-2202 (0, 1, 5, 12.5, 25, 50, 100, 200 μ M), and the mixture was then pre-incubated with enzyme samples to test their effects on PHGDH activity.

Flow Cytometric Analysis of Cell Cycle

MDA-MB-468 cells (300,000 cells/well) in exponential growth were plated into 6-well culture plates and then treated in triplicate with or without various concentrations of PKUMDL-WQ-2101 and PKUMDL-WQ-2201. After 24 hr, cells were harvested by trypsinization and centrifugation, and then washed twice with 1 \times PBS, fixed in 70% ice-cold ethanol, and kept at 4°C overnight. The fixed cells were then washed in 1 \times PBS and resuspended in 1 \times PBS containing 0.5% Triton X-100, 50 μ g/mL propidium iodide, and 50 μ g/mL DNase-free RNase A. The cell suspension was incubated in the dark for 30 min at 37°C and analyzed using a BD FACSCanto cytometer.

Generation of CRISPR-Cas9 PHGDH Knockout Cells

lentiCRISPR transfer plasmid (Addgene, plasmid no. 49535), lentiCRISPR-EGFP sgRNA 1 (Addgene, plasmid no. 51760), PMD2.G VSV-G envelope expressing plasmid (Addgene, plasmid no. 12259), and PsPAX2 lentiviral packaging plasmid (Addgene, plasmid no. 12260) were purchased. The target sequence of the sgRNA is GCTCTGAGCCTCCTTGGTGC (exon 8 of *PHGDH*). The plasmids were virally transfected into HEK293T cells using polyethylenimine (Polysciences) and transduced into SKOV3 cells as described previously (Shalem et al., 2014). Single-cell colonies of puromycin-resistant cells were selected and validated by western blotting.

Immunoblotting

Protein was extracted from cells using 1 \times radioimmunoprecipitation assay buffer (Rockland Immunochemicals) and centrifuged at 2,000 rpm for 30 min at 4°C. Protein concentrations were measured using Bradford protein assay (Bio-Rad) and loaded onto 7.5% SDS-PAGE gels transferred to polyvinylidene difluoride membranes. Membranes were blocked in 5% dry milk in Tris-buffered saline with Tween 20 and incubated with anti- β -actin (Cell Signaling Technology, 8H10D10) 1:2000 or anti-PHGDH (Sigma-Aldrich, WH0026227M1) 1:1000. Horseradish peroxidase-conjugated anti-mouse antibody (Rockland Immunochemicals, 611G4302), 1:2,000 was used as secondary antibody. Chemiluminescent signals were detected with a Clarity Western ECL Detection Kit (Bio-Rad) and imaged using a ChemiDoc MP system (Bio-Rad).

U - ^{13}C -Glucose Stable Isotope Labeling

SKOV3 cells (300,000 cells/well) were plated in a 6-well plate and allowed to adhere to the plate. Cells were then replaced with RPMI-1640 medium containing 11 mM U - ^{13}C -glucose (Cambridge Isotope Laboratories) and incubated for 24 hr. For U - ^{13}C -glucose tracing with drug treatments, cells were first treated with their corresponding compounds for 24 hr, followed by medium replacement with 11 mM U - ^{13}C -glucose and corresponding drug treatment. Metabolites were then extracted.

Metabolite Extraction

Metabolite extraction and subsequent LC-HRMS for polar metabolites of HCT116 cells were carried out using a Q Exactive Orbitrap Plus as described previously (Liu et al., 2014). For details, see the [Supplemental Experimental Procedures](#).

Peak Extraction and Data Analysis

Raw data collected from LC-Q Exactive Plus MS were processed on Sieve 2.0 (Thermo Scientific). Peak alignment and detection were performed according to the protocol described by Thermo Scientific. For a targeted metabolite analysis, the “peak alignment and frame extraction” method was applied. An input file of theoretical m/z and detected retention time of 197 known metabolites was used for targeted metabolite analysis with data collected in positive mode, while a separate input file of 262 metabolites was used for negative mode. m/z width was set to 10 ppm. The output file including detected m/z and relative intensity in different samples was obtained after data processing. If the lowest integrated mass spectrometer signal (MS intensity) was less than 1,000 and the highest signal was less than 10,000, then this metabolite was considered below the detection limit and excluded for further data analysis. If the lowest signal was less than 1,000, but the highest signal was more than 10,000, then a value of 1,000 was imputed for the lowest signals. Serine and glycine samples were normalized by comparing relative labeling of glucose-derived labeled metabolites from treated with vehicle samples. For all other samples, MID were calculated and samples were normalized by comparing the ratio of glucose-derived labeled metabolites to unlabeled metabolites within each sample. Quantitation and statistics were calculated using Microsoft Excel and GraphPad Prism 6.

MDA-MB-468 and MDA-MB-231 Xenograft Mouse Models

All animal experiments were performed in strict accordance with the regulations for the Administration of Affairs Concerning Experimental Animals approved by the State Council of People's Republic of China (11-14-1988). The animal study protocols were reviewed and approved by the Institutional Animal Care and Use Committee (IACUC) of Beijing Vital River Laboratory Animal Technology Limited Company (permit P2016024) and were performed in accordance with the relevant guidelines and regulations. The laboratory animal usage license number is SYXK (Beijing)-2012-0024, certified by Beijing Committee of Science and Technology. The animals were randomized, but the investigators were not blinded to the experimental conditions. For the PKUMDL-WQ-2101 and PKUMDL-WQ-2201 bioactivity assay in vivo, MDA-MB-468 or MDA-MB-231 cells were injected into the fourth mammary fat pad of NOD.CB17 SCID/J mice at 2×10^5 or 5×10^5 cells per injection site, respectively (Vital River Laboratory Animal Technology). For MDA-MB-468, when the average tumor volume reached 30 mm³, the mice were randomized into seven groups ($n = 5$): vehicle control (10% DMSO, 20% Kolliphor EL (EL), and 70% PBS, intraperitoneally [i.p.]); 20, 10, and 5 mg/kg/day PKUMDL-WQ-2101 or PKUMDL-WQ-2201 (i.p.), respectively. For MDA-MB-231, after the tumor was palpable, the mice were randomized into three groups ($n = 5$): vehicle control (10% DMSO, 20% EL, and 70% PBS, i.p.); 20 mg/kg/day PKUMDL-WQ-2101 (i.p.); 20 mg/kg/day PKUMDL-WQ-2201 (i.p.). The tumor volume was calculated using the formula width (mm)² \times length (mm) \times 0.5.

SUPPLEMENTAL INFORMATION

Supplemental Information includes Supplemental Experimental Procedures, five figures, and one table and can be found with this article online at <http://dx.doi.org/10.1016/j.chembiol.2016.11.013>.

AUTHOR CONTRIBUTIONS

L.L. and Q.W. conceived the project. Q.W., M.V.L., J.W.L., and L.L. designed the study and analyzed data. Q.W. performed allosteric site prediction and virtual screening studies, molecular cloning, mutagenesis, protein expression and purification experiments, enzymatic assays, SPR assays, cell-based assays, and in vivo studies. M.V.L. conducted CRISPR-Cas9 experiments, MTT assays, and breast cancer cell metabolomics. P.L., X.D., and Y.L. contributed to the chemical synthesis and purity analysis of the compounds. Q.W.,

M.V.L., J.W.L., and L.L. wrote the manuscript. All the authors discussed the results and contributed to the writing and editing of the manuscript.

ACKNOWLEDGMENTS

This project was supported in part by the Ministry of Science and Technology and the National Natural Science Foundation of China (grants 2015CB910300, 2016YFA0502303 and 21633001 to L.L.); by the NIH (grants R00CA168997 and R01CA193256 to J.W.L.), and a predoctoral fellowship award from the National Science Foundation (to M.V.L.) in the US. The authors thank Dr. Min Fang in the College of Life Sciences, Peking University, for his support and discussions on the cell-based studies. A provisional patent related to this study has been filed.

Received: April 7, 2016

Revised: July 15, 2016

Accepted: November 22, 2016

Published: December 29, 2016

REFERENCES

- Ainscough, E.W., Brodie, A.M., Denny, W.A., Finlay, G.J., Gothe, S.A., and Ranford, J.D. (1999). Cytotoxicity of salicylaldehyde benzoylhydrazone analogs and their transition metal complexes: quantitative structure-activity relationships. *J. Inorg. Biochem.* **77**, 125–133.
- Auld, D.S., Southall, N.T., Jadhav, A., Johnson, R.L., Diller, D.J., Simeonov, A., Austin, C.P., and Ingles, J. (2008). Characterization of chemical libraries for luciferase inhibitory activity. *J. Med. Chem.* **51**, 2372–2386.
- Baell, J.B., and Holloway, G.A. (2010). New substructure filters for removal of pan assay interference compounds (PAINS) from screening libraries and for their exclusion in bioassays. *J. Med. Chem.* **53**, 2719–2740.
- Beroukhi, R., Mermel, C.H., Porter, D., Wei, G., Raychaudhuri, S., Donovan, J., Barretina, J., Boehm, J.S., Dobson, J., Urashima, M., et al. (2010). The landscape of somatic copy-number alteration across human cancers. *Nature* **463**, 899–905.
- Birsoy, K., Wang, T., Possemato, R., Yilmaz, O.H., Koch, C.E., Chen, W.W., Hutchins, A.W., Gultekin, Y., Peterson, T.R., Carrette, J.E., et al. (2013). MCT1-mediated transport of a toxic molecule is an effective strategy for targeting glycolytic tumors. *Nat. Genet.* **45**, 104–108.
- Botham, R.C., Fan, T.M., Im, I., Borst, L.B., Dirikolu, L., and Hergenrother, P.J. (2014). Dual small-molecule targeting of procaspase-3 dramatically enhances zymogen activation and anticancer activity. *J. Am. Chem. Soc.* **136**, 1312–1319.
- Chen, J., Chung, F., Yang, G., Pu, M., Gao, H., Jiang, W., Yin, H., Capka, V., Kasibhatla, S., Laffitte, B., et al. (2013). Phosphoglycerate dehydrogenase is dispensable for breast tumor maintenance and growth. *Oncotarget* **4**, 2502–2511.
- Chou, T.C. (2006). Theoretical basis, experimental design, and computerized simulation of synergism and antagonism in drug combination studies. *Pharmacol. Rev.* **58**, 621–681.
- Clem, B.F., Clem, A.L., Yalcin, A., Goswami, U., Arumugam, S., Telang, S., Trent, J.O., and Chesney, J. (2011). A novel small molecule antagonist of choline kinase- α that simultaneously suppresses MAPK and PI3K/AKT signaling. *Oncogene* **30**, 3370–3380.
- DeNicola, G.M., Chen, P.H., Mullarky, E., Sudderth, J.A., Hu, Z., Wu, D., Tang, H., Xie, Y., Asara, J.M., Huffman, K.E., et al. (2015). NRF2 regulates serine biosynthesis in non-small cell lung cancer. *Nat. Genet.* **47**, 1475–1481.
- Ding, J., Li, T., Wang, X., Zhao, E., Choi, J.H., Yang, L., Zha, Y., Dong, Z., Huang, S., Asara, J.M., et al. (2013). The histone H3 methyltransferase G9A epigenetically activates the serine-glycine synthesis pathway to sustain cancer cell survival and proliferation. *Cell Metab.* **18**, 896–907.
- Fan, J., Ye, J., Kamphorst, J.J., Shlomi, T., Thompson, C.B., and Rabinowitz, J.D. (2014). Quantitative flux analysis reveals folate-dependent NADPH production. *Nature* **510**, 298–302.
- Friesner, R.A., Banks, J.L., Murphy, R.B., Halgren, T.A., Klicic, J.J., Mainz, D.T., Repasky, M.P., Knoll, E.H., Shelley, M., Perry, J.K., et al. (2004). Glide: a new approach for rapid, accurate docking and scoring. 1. Method and assessment of docking accuracy. *J. Med. Chem.* **47**, 1739–1749.
- Galluzzi, L., Kepp, O., Vander Heiden, M.G., and Kroemer, G. (2013). Metabolic targets for cancer therapy. *Nat. Rev. Drug Discov.* **12**, 829–846.
- Halgren, T.A., Murphy, R.B., Friesner, R.A., Beard, H.S., Frye, L.L., Pollard, W.T., and Banks, J.L. (2004). Glide: a new approach for rapid, accurate docking and scoring. 2. Enrichment factors in database screening. *J. Med. Chem.* **47**, 1750–1759.
- Hanahan, D., and Weinberg, R.A. (2011). Hallmarks of cancer: the next generation. *Cell* **144**, 646–674.
- Hart, C.E., Race, V., Achouri, Y., Wiame, E., Sharrard, M., Olpin, S.E., Watkinson, J., Bonham, J.R., Jaeken, J., Matthijs, G., et al. (2007). Phosphoserine aminotransferase deficiency: a novel disorder of the serine biosynthesis pathway. *Am. J. Hum. Genet.* **80**, 931–937.
- Kar, G., Keskin, O., Gursoy, A., and Nussinov, R. (2010). Allostery and population shift in drug discovery. *Curr. Opin. Pharmacol.* **10**, 715–722.
- Liu, X., Ser, Z., and Locasale, J.W. (2014). Development and quantitative evaluation of a high-resolution metabolomics technology. *Anal. Chem.* **86**, 2175–2184.
- Locasale, J.W. (2013). Serine, glycine and one-carbon units: cancer metabolism in full circle. *Nat. Rev. Cancer* **13**, 572–583.
- Locasale, J.W., Grassian, A.R., Melman, T., Lyssiotis, C.A., Mattaini, K.R., Bass, A.J., Heffron, G., Metallo, C.M., Muranen, T., Sharfi, H., et al. (2011). Phosphoglycerate dehydrogenase diverts glycolytic flux and contributes to oncogenesis. *Nat. Genet.* **43**, 869–874.
- Ma, L., Tao, Y., Duran, A., Llado, V., Galvez, A., Barger, J.F., Castilla, E.A., Chen, J., Yajima, T., Porollo, A., et al. (2013). Control of nutrient stress-induced metabolic reprogramming by PKC ζ in tumorigenesis. *Cell* **152**, 599–611.
- Ma, X., Meng, H., and Lai, L. (2016). Motions of allosteric and orthosteric ligand-binding sites in proteins are highly correlated. *J. Chem. Inf. Model.* **56**, 1725–1733.
- Mali, P., Yang, L., Esvelt, K.M., Aach, J., Guell, M., DiCarlo, J.E., Norville, J.E., and Church, G.M. (2013). RNA-guided human genome engineering via Cas9. *Science* **339**, 823–826.
- McGovern, S.L., Caselli, E., Grigorieff, N., and Shoichet, B.K. (2002). A common mechanism underlying promiscuous inhibitors from virtual and high-throughput screening. *J. Med. Chem.* **45**, 1712–1722.
- Meng, H., McClendon, C.L., Dai, Z., Li, K., Zhang, X., He, S., Shang, E., Liu, Y., and Lai, L. (2016). Discovery of novel 15-lipoxygenase activators to shift the human arachidonic acid metabolic network toward inflammation resolution. *J. Med. Chem.* **59**, 4202–4209.
- Mentch, S.J., Mehrmohamadi, M., Huang, L., Liu, X., Gupta, D., Mattocks, D., Gomez Padilla, P., Ables, G., Bamman, M.M., Thalacker-Mercer, A.E., et al. (2015). Histone methylation dynamics and gene regulation occur through the sensing of one-carbon metabolism. *Cell Metab.* **22**, 861–873.
- Merdanovic, M., Monig, T., Ehrmann, M., and Kaiser, M. (2013). Diversity of allosteric regulation in proteases. *ACS Chem. Biol.* **8**, 19–26.
- Mullarky, E., Lucki, N.C., Beheshti Zavareh, R., Anglin, J.L., Gomes, A.P., Nicolay, B.N., Wong, J.C., Christen, S., Takahashi, H., Singh, P.K., et al. (2016). Identification of a small molecule inhibitor of 3-phosphoglycerate dehydrogenase to target serine biosynthesis in cancers. *Proc. Natl. Acad. Sci. USA* **113**, 1778–1783.
- Nussinov, R., and Tsai, C.J. (2014). Unraveling structural mechanisms of allosteric drug action. *Trends Pharmacol. Sci.* **35**, 256–264.
- Ou, Y., Wang, S.J., Jiang, L., Zheng, B., and Gu, W. (2015). p53 Protein-mediated regulation of phosphoglycerate dehydrogenase (PHGDH) is crucial for the apoptotic response upon serine starvation. *J. Biol. Chem.* **290**, 457–466.
- Pacold, M.E., Brimacombe, K.R., Chan, S.H., Rohde, J.M., Lewis, C.A., Swier, L.J., Possemato, R., Chen, W.W., Sullivan, L.B., Fiske, B.P., et al. (2016). A PHGDH inhibitor reveals coordination of serine synthesis and one-carbon unit fate. *Nat. Chem. Biol.* **12**, 452–458.

- Pavlova, N.N., and Thompson, C.B. (2016). The emerging hallmarks of cancer metabolism. *Cell Metab.* **23**, 27–47.
- Pei, J., Yin, N., Ma, X., and Lai, L. (2014). Systems biology brings new dimensions for structure-based drug design. *J. Am. Chem. Soc.* **136**, 11556–11565.
- Possemato, R., Marks, K.M., Shaul, Y.D., Pacold, M.E., Kim, D., Birsoy, K., Sethumadhavan, S., Woo, H.K., Jang, H.G., Jha, A.K., et al. (2011). Functional genomics reveal that the serine synthesis pathway is essential in breast cancer. *Nature* **476**, 346–350.
- Qi, Y., Wang, Q., Tang, B., and Lai, L. (2012). Identifying allosteric binding sites in proteins with a two-state go model for novel allosteric effector discovery. *J. Chem. Theor. Comput.* **8**, 2962–2971.
- Shalem, O., Sanjana, N.E., Hartenian, E., Shi, X., Scott, D.A., Mikkelsen, T.S., Heckl, D., Ebert, B.L., Root, D.E., and Doench, J.G. (2014). Genome-scale CRISPR-Cas9 knockout screening in human cells. *Science* **343**, 84–87.
- Sonveaux, P., Vegrar, F., Schroeder, T., Wergin, M.C., Verrax, J., Rabbani, Z.N., De Saedeleer, C.J., Kennedy, K.M., Diepart, C., Jordan, B.F., et al. (2008). Targeting lactate-fueled respiration selectively kills hypoxic tumor cells in mice. *J. Clin. Invest.* **118**, 3930–3942.
- Turnbull, A.P., Salah, E., Savitsky, P., Gileadi, O., von Delft, F., Edwards, A., Arrowsmith, C., Weigelt, J., Sundstrom, M., Oppermann, U.. (2006). Crystal structure of human 3-phosphoglycerate dehydrogenase [online]. <http://dx.doi.org/10.2210/pdb2g76/pdb>. Available: <http://www.rcsb.org/pdb/explore/explore.do?structureId=2g76>.
- Unterlass, J.E., Basle, A., Blackburn, T.J., Tucker, J., Cano, C., Noble, M.E., and Curtin, N.J. (2016). Validating and enabling phosphoglycerate dehydrogenase (PHGDH) as a target for fragment-based drug discovery in PHGDH-amplified breast cancer. *Oncotarget*. <http://dx.doi.org/10.18632/oncotarget.11487>.
- Wagner, J.R., Lee, C.T., Durrant, J.D., Malmstrom, R.D., Feher, V.A., and Amaro, R.E. (2016). Emerging computational methods for the rational discovery of allosteric drugs. *Chem. Rev.* **116**, 6370–6390.
- Wang, Q., Qi, Y., Yin, N., and Lai, L. (2014). Discovery of novel allosteric effectors based on the predicted allosteric sites for *Escherichia coli* D-3-phosphoglycerate dehydrogenase. *PLoS One* **9**, e94829.
- Warburg, O. (1956). On the origin of cancer cells. *Science* **123**, 309–314.
- Yamada, K., Hara, N., Shibata, T., Osago, H., and Tsuchiya, M. (2006). The simultaneous measurement of nicotinamide adenine dinucleotide and related compounds by liquid chromatography/electrospray ionization tandem mass spectrometry. *Anal. Biochem.* **352**, 282–285.
- Yang, Q., Yang, Y., Li, L., Sun, W., Zhu, X., and Huang, Y. (2015). Polymeric nanomedicine for tumor-targeted combination therapy to elicit synergistic genotoxicity against prostate cancer. *ACS Appl. Mater. Inter.* **7**, 6661–6673.
- Yuan, Y., Pei, J., and Lai, L. (2011). LigBuilder 2: a practical de novo drug design approach. *J. Chem. Inf. Model.* **51**, 1083–1091.
- Yuan, Y., Pei, J., and Lai, L. (2013). Binding site detection and druggability prediction of protein targets for structure-based drug design. *Curr. Pharm. Des.* **19**, 2326–2333.
- Zhao, E., Ding, J., Xia, Y., Liu, M., Ye, B., Choi, J.H., Yan, C., Dong, Z., Huang, S., Zha, Y., et al. (2016). KDM4C and ATF4 cooperate in transcriptional control of amino acid metabolism. *Cell Rep.* **14**, 506–519.